A Linear Power Flow Formulation for Three-Phase Distribution Systems

Hamed Ahmadi, *Member, IEEE*, José R. Martí, *Life Fellow, IEEE*, and Alexandra von Meier, *Member, IEEE*

***Abstract*—Power flow analysis is one of the tools that is required in most of the distribution system studies. An important characteristic of distribution systems is the load unbalance in the phases and a three-phase power flow analysis is needed. In this paper, a three-phase linear power flow (3LPF) formulation is derived based on the fact that in a typical distribution system, voltage angles and magnitudes vary within relatively narrow boundaries. The accuracy of the proposed 3LPF is verified using several test cases. Potential applications of the proposed method are in distribution systems state estimation and volt-VAR optimization.**

***Index Terms*—Unbalanced power flow, voltage dependence.**

NOMENCLATURE

Y	Network admittance matrix.
G	Network conductance matrix.
B	Network susceptance matrix.
P, Q	Active/reactive power demand.
I	Load equivalent current injection.
$V^{\mathrm{re}}, V^{\mathrm{im}}$	Real/imaginary parts of nodal voltages.
$C^{\mathrm{Z}}, C^{\mathrm{I}}, C^{\mathrm{P}}$	ZIP load model parameters.
α	Tap position for voltage regulators.

I. INTRODUCTION

A. Motivation

THE modern Distribution Management System (DMS) provides decision support in near-real-time to optimize the performance of the system. Many of the computations done inside the DMS, such as state estimation, power flow analysis, volt-VAR optimization, network reconfiguration, etc., require power flow solutions. Since these computations need to be done at near-real-time, a fast and robust power flow solution method is needed. The authors have previously proposed the Linear Power Flow (LPF) formulation, assuming a balanced network [1]. This formulation is suitable for some of the optimization problems controlling three-phase equipment. For instance, when optimizing the network configuration, available switches are opened/closed to alter the network topology [2]. Since distribution system switches are often three-phase units (gang-operated), the LPF is an efficient alternative to other power flow analysis methods, e.g., the Newton-Raphson method, which are nonlinear and non-convex. In some cases, however, the unbalance between the phases cannot be neglected. For example, some of the voltage regulators are independent units installed on each phase. Distribution system state estimation (DSSE) also requires a full consideration of unbalances in the system model. In such cases, a three-phase power flow solution is needed.

The main purpose of this paper is to extend the application of the LPF method to unbalanced distribution systems. The 3LPF source codes are available to the power systems community under the GNU General Public License agreement at [3].

There are several well-known methods for power flow analysis in the literature. Newton-Raphson and Fast Decoupled are the most common methods for transmission systems, while the Backward/Forward Sweep is one of the widely used methods for distribution systems. There are, however, some key differences between transmission systems and distribution systems, such smaller X/R ratios, mixed overhead-underground cable sections, shorter lengths, phase unbalances, and often radial configuration and single point of supply. These special characteristics sometimes cause difficulties in applying conventional power flow analysis methods developed for transmission systems to distribution systems. Often, a balanced case is considered in distribution systems planning since the unbalances may not highly affect the decisions in the long-term planning stage. In addition, the computation time may not be an important factor in system planning studies. Therefore, the nonlinear and non-convex formulation of the balanced power flow problem is sufficient for most of the cases in system planning. When it comes to the near-real-time analysis and optimization, on the other hand, computation time and robustness become binding factors. The proposed 3LPF algorithm in this paper addresses these needs.

B. Related Literature

A three-phase version of the Newton-Raphson power flow analysis was formulated in [4] in complex form. Comparing the solution proposed in [4] with the balanced case revealed that this method takes 6 iterations to converge when the maximum

Manuscript received September 08, 2015; revised December 29, 2015; accepted February 15, 2016. Date of publication February 29, 2016; date of current version October 18, 2016. This work was supported by the National Science and Engineering Research Council (NSERC) of Canada. Paper no. TPWRS-01267-2015.

H. Ahmadi and J. R. Martí are with the Department of Electrical and Computer Engineering, The University of British Columbia, Vancouver, BC V6T 1Z4, Canada (e-mail: hameda@ece.ubc.ca; jrms@ece.ubc.ca).

A. von Meier is with the California Institute for Energy and Environment, University of California, Berkeley, CA 94704 USA (e-mail: vonmeier@ berkeley.edu).

Color versions of one or more of the figures in this paper are available online at http://ieeexplore.ieee.org.

Digital Object Identifier 10.1109/TPWRS.2016.2533540

tolerance is 10^{-5}, while the balanced case takes only 4 iterations to reach the same tolerance. Normally, optimization algorithms have difficulties with complex numbers and having the equations in complex form may not be suitable for optimization routines. The Fast-Decoupled method, when applied to distribution systems, may not perform well due to high R/X ratios in some cases. A method was proposed in [5] that uses a complex impedance base, as opposed to the conventional magnitude base, to calculate the per-unit impedances. By doing so, the R/X ratio can be deliberately altered to avoid convergence problems. This method has been shown to work for balanced networks in [5]. Sequence networks, namely the positive, negative, and zero sequences, were adopted in [6] and [7] to solve the unbalanced power flow. Sequence networks have some advantages in modeling DGs and transformers of various configurations [8] in the power flow framework.

The Backward/Forward Sweep method, originally developed for radial systems, was improved in [9] and [10] to account for networks with loops and laterals. A load-stepping technique was proposed in [11] to address the convergence issue of sweep-based methods in heavily loaded feeders. It should be noted that the sweep-based methods do not admit a closed form formulation of the power flow problem to be embedded in an optimization algorithm. Three methods were compared in [12] in terms of computational burden, namely the Newton, Dishonest Newton, and Fixed-Point Iteration (FPI) methods. A modified-augmented-nodal analysis method was used to construct the system of power flow equations. It was shown that the FPI method is faster than other competitors, especially the Forward/Backward Sweep method. In the FPI method of [12], loads are first represented as parallel R-L elements at the nominal voltage and in the consecutive iterations, appropriate current injections are added to the right-hand side to compensate for the mismatch.

The implicit Z_{Bus} Gauss method was introduced in [13] for power flow analysis. Loads and capacitor banks are replaced by equivalent current injections and a fixed admittance matrix is then factorized once to find the solution of a system of linear equations for which only the right-hand side changes at each iteration. Branch voltages, i.e., the difference between the voltages at the two ends of a branch, were taken as state variables to form the power flow equations in [14]. By doing so, the authors of [14] reached better performance than the implicit Z_{Bus} method.

The current injection method (CIM) for power flow analysis was previously proposed by the authors of [15] for single-phase balanced systems and was extended to the three-phase unbalanced cases in [16]. The CIM was adopted in [17], considering loops in the network instead of nodes, to form the power flow equations. The CIM was also employed in [18] and the impedance matrix was formed using an upper triangular matrix that relates the branch currents to nodal current injections.

There have been a few linear approximations of power flow equations in the literature. One linear approximation is the so-called DC power flow, in which all voltage magnitudes are assumed to be one per-unit, line resistances are ignored, and voltage angles are assumed to be small. In a DC power flow model, only active power flows can be approximated and reactive power flows are not considered [19]. The assumptions of DC power flow does not hold for a typical distribution system since the resistive and reactive parts of the line impedances are comparable. One recent study proposed the linearization of the nonlinear power flow manifold [20]. The power flow equations are linearized around the no-load solution using a first-order approximation method in [20]. A linear power flow approximation for a balanced distribution system was proposed in [21] which introduces a relatively large error in the solution but provides an upper and lower bound on nodal voltages.

In this paper, two methods are discussed for power flow analysis. The first method, which is based on the fixed-point iteration method, was obtained by slight modifications to the previously proposed current injection method and is discussed for comparison purposes only. The second method, called the 3LPF, is the main contribution of this paper and is a linear approximation of the first method. A modified version of the CIM is described that does not require the formation and updating of the coefficient matrix at every iteration. This method is used later as a reference to determine the error of the 3LPF. The modified version of the CIM used here was inspired by the implicit Z_{Bus} method of [13]. The algorithm starts by replacing loads by their equivalent complex current injection. At every iteration, the corresponding current injections are updated according to the nodal voltages calculated in the previous iteration. This way, the coefficient matrix of the system of linear equations is constant at all iterations and, therefore, the computational requirements are reduced. This is an FPI method for solving the power flow problem using the CIM. The FPI-based CIM is used as a reference to calculate the error of the 3LPF solution proposed in this paper.

The rest of the paper is organized as follows. In Section II, the FPI-based CIM for three-phase power flow analysis is described. The derivation of the 3LPF is explained in Section III. Simulation results are provided in Section IV, demonstrating the accuracy of the 3LPF solution. The main findings of this study are summarized in Section VI.

II. The Classical Current Injection Method

A. Branch Models

Distribution systems involve three-phase, double-phase, and single-phase branches and loads. Four-wire sections can be replaced by their three-phase equivalent obtained by applying Kron's reduction technique [13]. The branch admittance matrix can be found by taking the inverse of the branch impedance matrix. The line capacitance (also referred to as line charging) can be considered based on the π-model representation of the line. Half of the line total capacitance is added to one end and the other half to the other end.

B. Load Models

The analysis in this paper is limited to the primary distribution system, i.e., from the substation transformer to the distribution transformers. There is usually minimal information available to the utilities regarding the secondary distribution system in terms of exact load values, length and type of service cables, etc. A

common practice is to assume a typical voltage drop on the secondary system and limit the power flow analysis to the primary distribution system. Loads may appear in Y or Δ connections. When loads are connected in Y-grounded, the equivalent current injection in complex form can be calculated as:

$$\bar{I}_{\rm ph} = \left(\frac{P_{\rm ph} + j\, Q_{\rm ph}}{V^{\rm re}_{\rm ph} + j\, V^{\rm im}_{\rm ph}} \right)^* \tag{1}$$

where ph $\in \{A, B, C\}$ stands for the phases. In rectangular coordinates, (1) can be expressed as:

$$I^{\rm re}_{\rm ph} = \frac{P_{\rm ph}\, V^{\rm re}_{\rm ph} + Q_{\rm ph}\, V^{\rm im}_{\rm ph}}{\left|V^{\rm re}_{\rm ph}\right|^2 + \left|V^{\rm im}_{\rm ph}\right|^2}, I^{\rm im}_{\rm ph} = \frac{P_{\rm ph}\, V^{\rm im}_{\rm ph} - Q_{\rm ph}\, V^{\rm re}_{\rm ph}}{\left|V^{\rm re}_{\rm ph}\right|^2 + \left|V^{\rm im}_{\rm ph}\right|^2} \tag{2}$$

Loads are voltage-dependent elements. Conventionally, the voltage dependence of loads is characterized by the so-called ZIP model, given by

$$P_{\rm ph} = C^Z_{\rm ph} \left(\frac{V_{\rm ph}}{V^0_{\rm ph}} \right)^2 + C^I_{\rm ph} \left(\frac{V_{\rm ph}}{V^0_{\rm ph}} \right) + C^P_{\rm ph} \tag{3a}$$

$$Q_{\rm ph} = \tilde{C}^Z_{\rm ph} \left(\frac{V_{\rm ph}}{V^0_{\rm ph}} \right)^2 + \tilde{C}^I_{\rm ph} \left(\frac{V_{\rm ph}}{V^0_{\rm ph}} \right) + \tilde{C}^P_{\rm ph} \tag{3b}$$

where the parameters $C_{\rm ph}$ are obtained using a curve-fitting technique. Some typical values for these parameters were obtained in, e.g., [22], for different load types. For instance, a heater can be modeled as $C^Z = 1$, with other parameters equal to zero. Values for $P_{\rm ph}$ and $Q_{\rm ph}$ in (3) are substituted in (2), rendering the current injections as functions of the real and imaginary parts of the corresponding nodal voltages.

Modeling of the Y-connected loads is straight forward. However, in some cases loads are connected in Δ configuration, as in Fig. 1(a). In such cases, equivalent current injections for each phase can be obtained using the following equation:

$$\begin{bmatrix} \bar{I}_A \\ \bar{I}_B \\ \bar{I}_C \end{bmatrix} = \begin{bmatrix} 1 & 0 & -1 \\ -1 & 1 & 0 \\ 0 & -1 & 1 \end{bmatrix} \begin{bmatrix} \bar{I}_{ab} \\ \bar{I}_{bc} \\ \bar{I}_{ca} \end{bmatrix} \tag{4}$$

where

$$\bar{I}_{ab} = \left(\frac{P_{ab} + j\, Q_{ab}}{V^{\rm re}_{ab} + j\, V^{\rm im}_{ab}} \right)^* \tag{5}$$

and similar equations can be written for $\bar{I}_{bc}$ and $\bar{I}_{ca}$. Using these equivalent current injections, a Δ-connected load can be represented by Y-connected current sources. Note that the sum of these three currents is zero, which immediately follows from (4). Load voltage dependence can also be considered for Δ-connected loads. The voltages in this case are line-to-line voltages.

Distributed generation units can be modeled in the 3LPF framework as either constant-power (power factor control) or constant-current elements (negative loads). The current version of the 3LPF is not able to model PV nodes (voltage-controlled nodes) in the network.

C. Ideal Voltage Regulator

Fig. 2 shows the diagram of a Y-connected voltage regulator. Due to the daily and seasonal load variation, feeder voltage profiles need to be regulated to ensure all voltages along the feeder are within the standard range. Also, voltage drop on long feeders may exceed the standard values and a voltage regulator can be placed in an appropriate location to adjust the voltage. A common type of voltage regulator is the Y-connected type, with independent operation on each phase. The voltage buck/boost level applied by an ideal regulator to each phase is shown by $\alpha_{\rm ph}$ here, which is the ratio of the secondary voltage over the primary voltage, i.e., $\alpha_{\rm ph} = |\bar{V}^s_{\rm ph}|/|\bar{V}^p_{\rm ph}|$. When the line drop compensation (LDC) is activated, the control mechanism of the regulator adjusts the voltage magnitude at an electrical distance, given by the user-defined values for $R^{\rm LDC}_{\rm ph}$ and $X^{\rm LDC}_{\rm ph}$ for each phase. Therefore, the monitored voltage for each phase is $\bar{V}^s_{\rm ph} - (R^{\rm LDC}_{\rm ph} + j\, X^{\rm LDC}_{\rm ph})\, \bar{I}^s_{\rm ph}$.

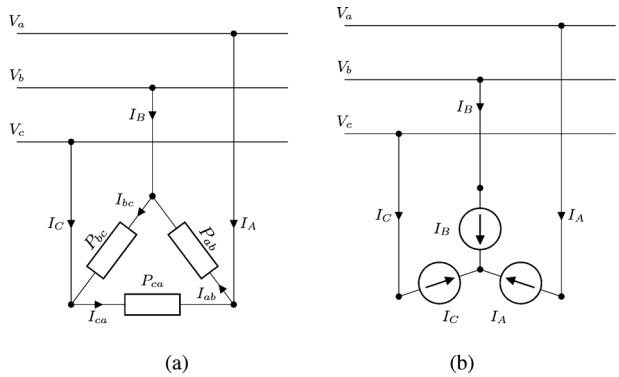

Fig. 1. A Δ-connected load and its equivalent Y-connected current injection. (a) Δ-connected load, (b) Equivalent current injection.

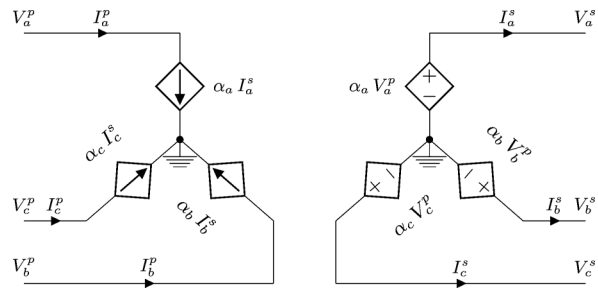

Fig. 2. The equivalent model of a Y-connected voltage regulator.

In order to consider the regulator model within the nodal analysis, the primary and secondary sides are treated as separate nodes. Dependent current sources are added to the Kirchhoff's Current Law (KCL) equations written for the primary node. Extra variables are then introduced to the problem, i.e., $\bar{I}^s_{\rm ph}$, and extra equations for $\bar{V}^p_{\rm ph}$. The new admittance matrix is sometimes referred to as the augmented admittance matrix.

An alternative method for modeling voltage regulators was discussed in [23], in which voltage buck/boost control is imposed by appropriate current injections at each end. Any other component which can be modeled as current injections or equivalent series/shunt admittance can be incorporated into the 3LPF framework. Modeling aspects of different transformer configurations within the power flow algorithm have been discussed in [24]. These models can be readily incorporated into the 3LPF framework since they are based on the admittance matrix representation of the system.

D. Fixed-Point Iteration

The current injection method (CIM) is based on applying the KCL at each node in the system. The sum of the currents drawn from a node by the loads should be equal to the sum of the currents injected into that node from the rest of the network. Using load equivalent current injections, the following general formulation can be reached for a system with n nodes (including all the existing phases):

$$\bar{Y}\,\bar{V} = \bar{I}(\bar{V}) \tag{6}$$

where $\bar{Y} \in \mathbb{C}^{n\times n}$ is the admittance matrix; $\bar{I}(\bar{V}) \in \mathbb{C}^n$ is the load equivalent current injections as a nonlinear function of the nodal voltages $\bar{V} \in \mathbb{C}^n$. Starting from an initial guess $\bar{V}_0$, under the condition that $\bar{Y}$ is invertible, (6) can be treated as a fixed-point iteration (FPI) problem. The iteration method is described in Algorithm 1. The process continues until the difference between the two consecutive solutions is less than the predefined tolerance ϵ.

Algorithm 1 CIM using Fixed-Point Iteration

1: **procedure** FIXED-POINT ITERATION
2: k = 0
3: **while** $E \geq \epsilon$ **do**
4: Update current injections $\bar{I}(\bar{V}_k)$
5: Solve $\bar{Y}\,\bar{V} = \bar{I}(\bar{V})$ for $\bar{V}_{k+1}$
6: $E = \|\bar{V}_{k+1} - \bar{V}_k\|$
7: $k = k + 1$
8: **end while**
9: **end procedure**

The nodal voltages in the unloaded case are considered as the initial guess, i.e., all the voltages are equal to the substation voltage. The FPI algorithm used here is different from the one used in [12] in the sense that loads are converted to R-L equivalents in [12] while they are considered as equivalent current injections here. As reported in [12], the FPI method is about three times faster than the Newton method and about two times faster than the Dishonest Newton method for the IEEE 8500-Node system.

III. THE LINEAR POWER FLOW METHOD

The CIM, compared to the Newton-Raphson equations, takes the complexity and nonlinearities from the power flow equations and places them in the load modeling part. It is more effective to perform linearization on the load models where the impacts on the solution accuracy are relatively small. Having a closer look at (6) reveals that the only nonlinearity arises from the right-hand side of the equations, i.e., the equivalent current injections $\bar{I}(\bar{V})$. Since (6) is written in complex form, a decomposed version is considered here which is in the real form:

$$\begin{bmatrix} G & -B \\ B & G \end{bmatrix} \begin{bmatrix} V^{\mathrm{re}} \\ V^{\mathrm{im}} \end{bmatrix} = \begin{bmatrix} I^{\mathrm{re}}(V^{\mathrm{re}}, V^{\mathrm{im}}) \\ I^{\mathrm{im}}(V^{\mathrm{re}}, V^{\mathrm{im}}) \end{bmatrix} \tag{7}$$

in which $G \in \mathbb{R}^{n\times n}$ and $B \in \mathbb{R}^{n\times n}$ are the real and imaginary parts of the augmented admittance matrix $\bar{Y}$; $V^{\mathrm{re}} \in \mathbb{R}^n$ and $V^{\mathrm{im}} \in \mathbb{R}^n$ are the real and imaginary parts of the three-phase nodal voltages $\bar{V}$, respectively; $I^{\mathrm{re}} \in \mathbb{R}^n$ and $I^{\mathrm{im}} \in \mathbb{R}^n$ are the real and imaginary parts of the three-phase nodal current injections $\bar{I}(\bar{V})$, respectively. The terms in the right-hand side of (7) were derived in (2) for Y-connected loads and can be similarly derived for Δ-connected loads using (4) and (5). Using these equivalents for I^{re} and I^{im}, all the nonlinear terms turn out to be functions of $V^{\mathrm{re}}_{\mathrm{ph}}$ and $V^{\mathrm{im}}_{\mathrm{ph}}$. Substituting the corresponding values of P_{ph} and Q_{ph} from (3) into (2), and assuming $V^0_{\mathrm{ph}} = 1$ p.u., the relations in (8a) and (8b), shown at the bottom of the page, can be derived.

Depending on the load voltage dependence characteristics, four nonlinear terms appear in (8), as follows:

$$f_{1,\mathrm{ph}} = \frac{V^{\mathrm{re}}_{\mathrm{ph}}}{|V^{\mathrm{re}}_{\mathrm{ph}}|^2 + |V^{\mathrm{im}}_{\mathrm{ph}}|^2}, f_{2,\mathrm{ph}} = \frac{V^{\mathrm{im}}_{\mathrm{ph}}}{|V^{\mathrm{re}}_{\mathrm{ph}}|^2 + |V^{\mathrm{im}}_{\mathrm{ph}}|^2} \tag{9a}$$

$$f_{3,\mathrm{ph}} = \frac{V^{\mathrm{re}}_{\mathrm{ph}}}{\sqrt{|V^{\mathrm{re}}_{\mathrm{ph}}|^2 + |V^{\mathrm{im}}_{\mathrm{ph}}|^2}}, f_{4,\mathrm{ph}} = \frac{V^{\mathrm{im}}_{\mathrm{ph}}}{\sqrt{|V^{\mathrm{re}}_{\mathrm{ph}}|^2 + |V^{\mathrm{im}}_{\mathrm{ph}}|^2}} \tag{9b}$$

These nonlinear functions $f_{i,\mathrm{ph}}$ can be approximated with their linear equivalents using a curve-fitting technique when $V^{\mathrm{re}}_{\mathrm{ph}}$ and $V^{\mathrm{im}}_{\mathrm{ph}}$ vary within a certain range. The approximated linear functions $\hat{f}_{i,\mathrm{ph}}$ are then expressed as

$$\hat{f}_{i,\mathrm{ph}} = K^{\mathrm{ph}}_{1i} V^{\mathrm{re}} + K^{\mathrm{ph}}_{2i} V^{\mathrm{im}} + K^{\mathrm{ph}}_{3i}, i \in \{1,2,3,4\} \tag{10}$$

$$I^{\mathrm{re}}_{\mathrm{ph}} = C^Z_{\mathrm{ph}} V^{\mathrm{re}}_{\mathrm{ph}} + C^I_{\mathrm{ph}} \frac{V^{\mathrm{re}}_{\mathrm{ph}}}{\sqrt{|V^{\mathrm{re}}_{\mathrm{ph}}|^2 + |V^{\mathrm{im}}_{\mathrm{ph}}|^2}} + C^P_{\mathrm{ph}} \frac{V^{\mathrm{re}}_{\mathrm{ph}}}{|V^{\mathrm{re}}_{\mathrm{ph}}|^2 + |V^{\mathrm{im}}_{\mathrm{ph}}|^2} +$$
$$\hat{C}^Z_{\mathrm{ph}} V^{\mathrm{im}}_{\mathrm{ph}} + \hat{C}^I_{\mathrm{ph}} \frac{V^{\mathrm{im}}_{\mathrm{ph}}}{\sqrt{|V^{\mathrm{re}}_{\mathrm{ph}}|^2 + |V^{\mathrm{im}}_{\mathrm{ph}}|^2}} + \hat{C}^P_{\mathrm{ph}} \frac{V^{\mathrm{im}}_{\mathrm{ph}}}{|V^{\mathrm{re}}_{\mathrm{ph}}|^2 + |V^{\mathrm{im}}_{\mathrm{ph}}|^2} \tag{8a}$$

$$I^{\mathrm{im}}_{\mathrm{ph}} = C^Z_{\mathrm{ph}} V^{\mathrm{im}}_{\mathrm{ph}} + C^I_{\mathrm{ph}} \frac{V^{\mathrm{im}}_{\mathrm{ph}}}{\sqrt{|V^{\mathrm{re}}_{\mathrm{ph}}|^2 + |V^{\mathrm{im}}_{\mathrm{ph}}|^2}} + C^P_{\mathrm{ph}} \frac{V^{\mathrm{im}}_{\mathrm{ph}}}{|V^{\mathrm{re}}_{\mathrm{ph}}|^2 + |V^{\mathrm{im}}_{\mathrm{ph}}|^2} -$$
$$\hat{C}^Z_{\mathrm{ph}} V^{\mathrm{re}}_{\mathrm{ph}} - \hat{C}^I_{\mathrm{ph}} \frac{V^{\mathrm{re}}_{\mathrm{ph}}}{\sqrt{|V^{\mathrm{re}}_{\mathrm{ph}}|^2 + |V^{\mathrm{im}}_{\mathrm{ph}}|^2}} - \hat{C}^P_{\mathrm{ph}} \frac{V^{\mathrm{re}}_{\mathrm{ph}}}{|V^{\mathrm{re}}_{\mathrm{ph}}|^2 + |V^{\mathrm{im}}_{\mathrm{ph}}|^2} \tag{8b}$$

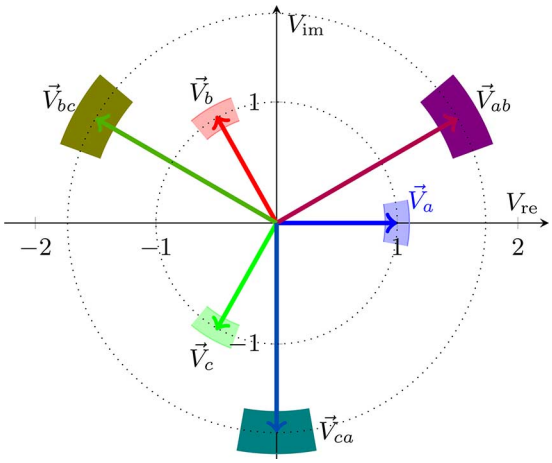

Fig. 3. Ranges of variation for phase and phase-to-phase voltages for ±10% change in magnitudes and ±10 degrees change in the angles.

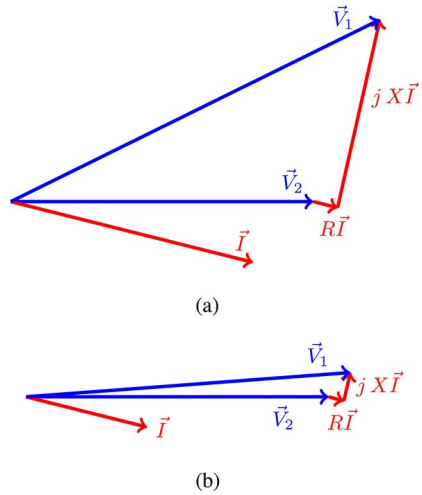

Fig. 4. Phasor diagram of voltages in a two-bus system for a typical transmission and distribution line. (a) Transmission System, (b) Distribution System.

The linearization process for $f_{i,\text{ph}}$ is explained in Appendix A. The parameters K_{1i}^{ph} and K_{2i}^{ph} are taken to the left-hand side and added to the appropriate elements in the coefficient matrix in (7). The resulting system of linear equations yields the exact solution when all the loads are modeled as constant-impedance. In other cases, a small error is introduced. The error associated with these approximations is evaluated in Section IV for different scenarios.

The nonlinear terms for Δ-connected loads need to be further elaborated on. The terms resulting from decomposing (5) into its real and imaginary parts have phase-to-phase voltages as variables rather than phase-to-ground voltages. In this case, the variables x and y in Appendix A are, e.g., V_{ab}^{re} and V_{ab}^{im}, respectively. The phase-to-phase voltages can then be expressed as the difference between the corresponding phase-to-ground voltages, e.g., $V_{ab}^{\text{re}} = V_a^{\text{re}} - V_b^{\text{re}}$. The domains of variation for each phase voltage and phase-to-phase voltage are shown in Fig. 3. The filled areas show the variation of the arrow tips for each variable. Phase voltage magnitudes are assumed to vary ±12% and the phase angles to vary ±10 degrees.

It is important to notice the difference between a linear approximation of a function obtained at one point using its first derivative (truncated Taylor series expansion) and its linear approximation over a bounded domain centered by that same point. For example, consider $f(x) = x^3, 0 < x < 1$. The first-order approximation of f obtained around $x = 0.5$ is $0.75x - 0.25$ and its linear approximation within this range is $0.9x - 0.2$. The sum of squared errors for these approximations over the given domain are 3.2 and 1.35, respectively. This also helps understanding the difference between using the Jacobian matrix versus the linearization technique applied here. The first-order approximation of a nonlinear function is only valid for a small variation around an operating point, whereas a linearized version over a bounded region allows for larger variations of variables by distributing the approximation error over the given region [25].

A. Transmission Systems Versus Distribution Systems

The Canadian Standard Association (CSA) indicates the voltage ranges for normal operation and extreme conditions, as given in Table I. Based on these values, the range of voltage variation used in the linearizations is justifiable. To understand the range of variation of the voltage angle, a simple example is analyzed here. Assume a load connected to a source via an impedance. The vector diagrams of voltages and currents for this simple two-bus system are shown in Fig. 4.

TABLE I
STANDARD VOLTAGE RANGES FOR DISTRIBUTION SYSTEMS [26]

	$V_{\text{min}}(\%)$	$V_{\text{max}}(\%)$
Normal Operating Range	-8	+4
Extreme Operating Range	-12	+6

It is important to understand the differences between a transmission system and a distribution feeder. In a transmission system, lines are usually long with high X/R ratio. Also, the amount of power being transferred through the line is relatively large. In a distribution feeder, on the other hand, lines are shorter with smaller X/R ratio and the amount of power being transferred is relatively small. A common base for voltage and power is used to find the per-unit values of the parameters shown in Fig. 4. As can be seen, voltage angles are smaller in distribution systems. Voltage angles depend on the value of load and its power factor as well as the length of the line and its X/R ratio. The considered ranges for voltage angles and magnitudes are derived here based on studying several operating conditions and line configurations typical for distribution feeders.

Another important difference between transmission and distribution systems is related to the voltage drop contribution from the resistive and reactive parts of the line impedances. As shown in Fig. 4, voltage drop is mostly caused by the line reactance in a transmission system while both the line resistance and reactance contribute to the voltage drop in a distribution system. This is one of the reasons for the DC power flow method not to be applicable to distribution systems.

IV. Simulation Results

In order to demonstrate the performance of the 3LPF, a simple 3-Node test system is used here. This system is shown in Fig. 5.

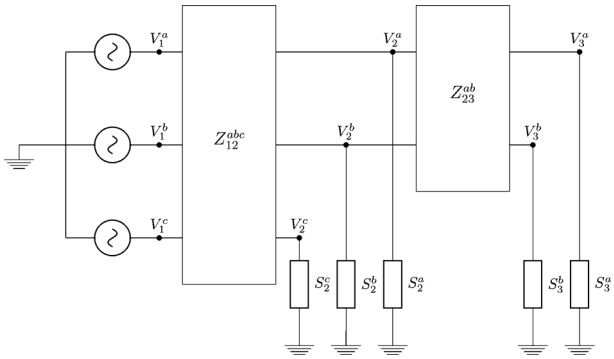

Fig. 5. The 3-Node test system.

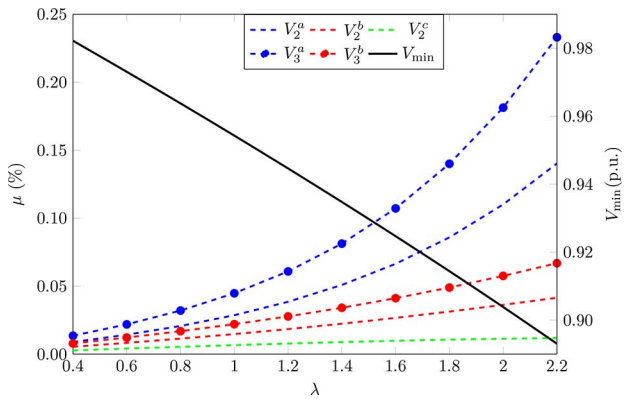

Fig. 6. Relative error of the 3LPF for different feeder loadings.

The branch impedances and loads are given in Appendix C. Several parameters can affect the accuracy of the 3LPF, including the R/X ratio, length of the lines, feeder loading (λ), load power factor ($\cos(\phi)$), and load voltage dependence (Z, I, and P portions). The errors associated with the 3LPF results are calculated with respect to the results obtained using the CIM method. Let the voltage magnitudes obtained by the 3LPF be V_{LPF} and those obtained by the CIM be V_{CIM}. The relative error, μ in %, is then calculated as

$$\mu = 100 \times \frac{|V_{\text{CIM}} - V_{\text{LPF}}|}{V_{\text{CIM}}} \tag{11}$$

In each simulation, only one factor is altered and other parameters are fixed at the original values given in Appendix C. The first parameter to be considered is the feeder loading, which is altered by scaling the load P and Q by a factor λ. Fig. 6 shows the errors for each node in the system. In the same figure, the system minimum voltage is also shown on the right vertical axis. The loads are scaled up until the minimum voltage falls below 0.90 per-unit. The maximum error in this case is less than 0.24%, associated with Phase A at Node 3. With normal feeder loading, i.e., $\lambda = 1$, the maximum error is less than 0.05%. It is worthwhile mentioning that the unbalance caused by the non-existing phase C at Node 3 contributed significantly to the voltage unbalance, about 5% difference in magnitudes in phases A and B, urging the application of a three-phase analysis.

The effect of the load power factor, $\cos(\phi)$, is shown in Fig. 7. Here, the value of load active power is kept fixed and the reactive power is determined based on the value of ϕ in Fig. 7. For

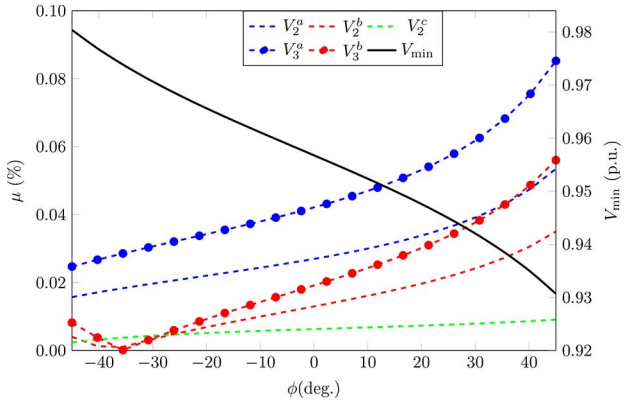

Fig. 7. Relative error of the 3LPF versus loads power factor.

instance, $\phi = 0$, $\phi = \pi/4$, and $\phi = -\pi/4$ correspond to $Q = 0$, $Q = P$ lagging, and $Q = -P$ leading, respectively. The maximum error in this case is about 0.09%. As the load becomes more capacitive (negative values for ϕ), the voltage magnitudes get closer to 1 p.u., increasing the accuracy of the 3LPF solution.

Loads are voltage-dependent elements, i.e., the amount of active and reactive power demand changes as the voltage level varies. In the standard IEEE test systems, loads are modeled as constant-impedance (Z), constant-current (I), or constant-power (PQ) [27]. The errors of the 3LPF solution for these three cases are shown in Fig. 8. All loads, including their active and reactive power components, are assumed to have the same voltage dependence in these simulations. Note that the 3LPF is capable of modeling any combinations of components of the ZIP model described in (3). The highest error occurs for the constant-power load model and the error of the constant-impedance model is zero.

The R/X ratio of the branches varies in distribution systems, depending on the phase arrangement, type of conductors, overhead lines or underground cables, voltage levels, etc. The values for X are kept constant in the test system and the values for R are calculated based on the R/X ratio. It should be noted that all the 9 elements of the three-phase resistance matrices are scaled by the given R/X factor. The impact of the R/X ratio on the error of the 3LPF solution is shown in Fig. 9. The maximum error in this case is about 0.11%.

The feeder length is another important factor that can impact the error of the 3LPF solution. The effect of the feeder length on the accuracy of the 3LPF solution is shown in Fig. 10. The feeder length is increased to the point that the maximum voltage drop almost exceeds the standard limits. In this case, the maximum error is about 0.16%. Due to the relatively large hypothetical values chosen for the line parameters, the voltage limits are reached at 6 km. This happens while the voltage angles deviate from the nominal values, i.e., $(0°, -120°, 120°)$, by less than $3°$. Adding a voltage regulator brings the voltage magnitudes within the standard limits, and the voltage angles may grow larger. In our approximations, $\pm 10°$ is considered for voltage angles, which was derived based on numerous analyses of real and hypothetical distribution systems.

The IEEE 13-Node, the IEEE 123-Node, and the IEEE 8500-Node test systems, described in [27] and [28], are also used

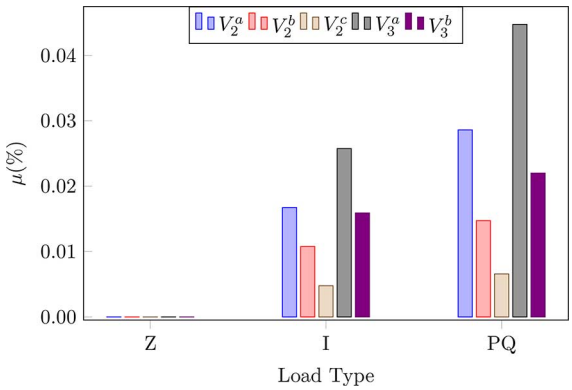

Fig. 8. Relative error of the 3LPF versus loads voltage dependence.

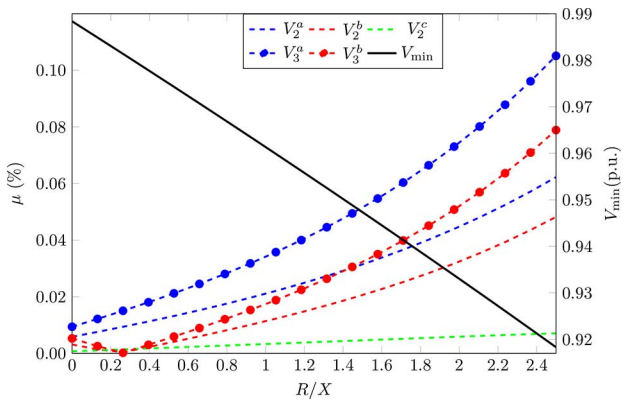

Fig. 9. Relative error of the 3LPF versus R/X ratio of lines.

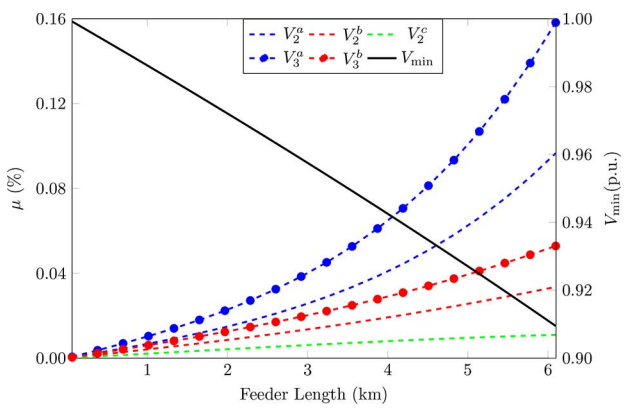

Fig. 10. Relative error of the 3LPF versus feeder length.

here to evaluate the accuracy of the 3LPF solution. The following modifications are made to the IEEE 13-Node system: Transformer XFM-1 is replaced by a 3000 ft long L602 line; The distributed load between Nodes 632 and 671 is assumed to be connected at Node 632. The power flow solution for this test system is provided in Table II. The histogram of error μ given by (11), considering all the phases and nodes, is shown in Fig. 12. The error in this case is less than 0.03%. This system was also adopted in [20] to numerically evaluate their proposed linearization method, referred to as the 1st Order method here. A comparison is made in terms of the solution accuracy between the 3LPF and the 1st Order method. Fig. 11 shows the error for each node and phase. In the first scenario, shown in Fig. 11(a),

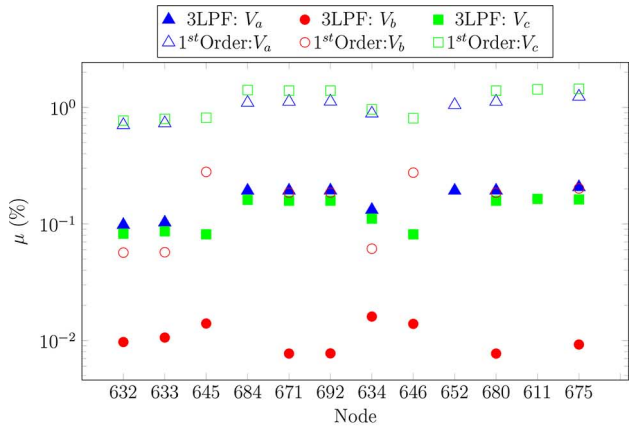

(a)

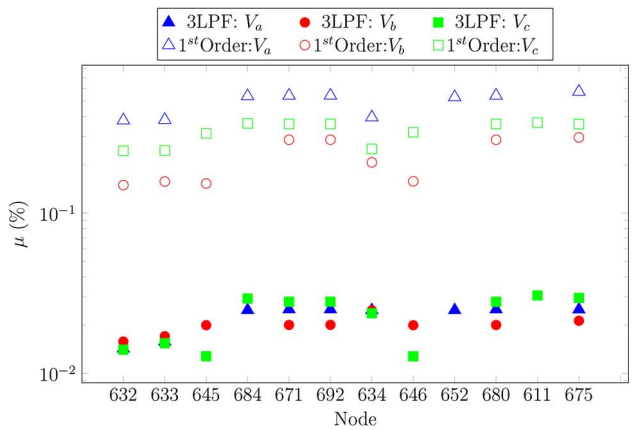

(b)

Fig. 11. Relative error of power flow solutions obtained by the 1st Order method of [20] and the 3LPF for the IEEE 13-Node system. (a) Tap changer set at $\{1.0625, 1.05, 1.0687\}$, (b) Tap changer set at $\{1, 1, 1\}$.

the voltage regulator taps are adjusted at [1.0625, 1.05, 1.0687]. The maximum relative errors (μ) in this case for the 1st Order method and the 3LPF are 0.57% and 0.03%, respectively. In the second scenario, shown in Fig. 11(b), the tap changer is set at [1, 1, 1]. The maximum μ in this case is 1.44% and 0.21% for the 1st Order method and the 3LPF, respectively.

In the IEEE 123-Node system, the transformer between nodes 61 and 610 is removed. The histogram of error μ for this system is shown in Fig. 12. The error in this case does not exceed 0.025%.

The IEEE 8500-Node system is described in [28]. The total load in the system is about 10.8 MW + 2.7 MVAR. This system consists of the primary network (12.47 kV), single-phase distribution transformers (7.2 kV/120 V/120 V), and a 50-ft service cable that connects the loads to the customer service transformers. In this study, only the primary network is considered. The primary network consists of about 3680 nodes. The customer service transformers are replaced by the equivalent load connected to them. Voltage regulators are set at tap 1.02 on all phases and are kept fixed. There are four capacitor banks, all of which are assumed to be connected since the given loading is for peak load conditions. The histogram of error μ for this system is shown in Fig. 12. The error in this case does not exceed 0.06%.

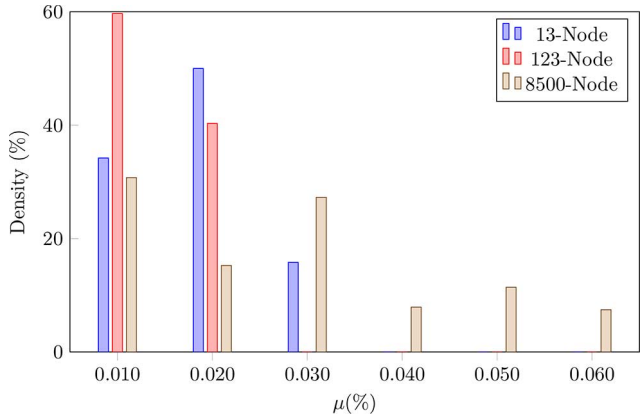

Fig. 12. Histogram of relative error of the 3LPF solution for the IEEE 13-, 123-, and 8500-Node systems, considering all phases at each node.

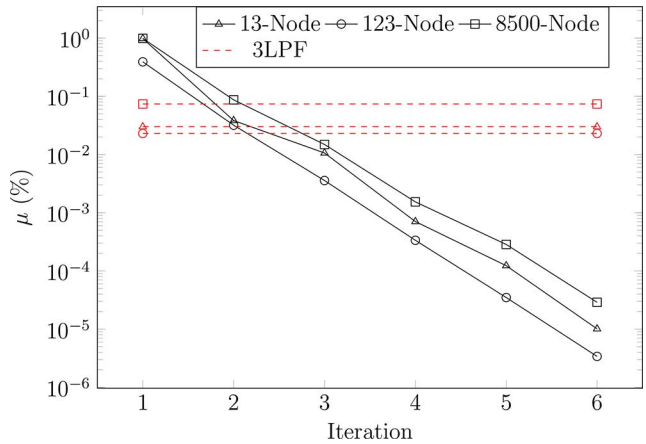

Fig. 13. Maximum error in voltage magnitudes per iteration for the CIM solution for the IEEE 13, 123, and 8500-Node test systems. The 3LPF error is shown using a red dashed line.

TABLE II
POWER FLOW SOLUTION FOR THE IEEE 13-NODE TEST SYSTEM OBTAINED BY THE 3LPF

Node	V_a	V_b	V_c	δ_a	δ_b	δ_c
650	1	1	1	0	-120	120
VR	1.062	1.050	1.069	0.00	-120.00	120.00
632	1.021	1.042	1.018	-2.48	-121.73	117.83
633	1.018	1.040	1.015	-2.55	-121.77	117.82
634	1.015	1.038	1.013	-2.61	-121.81	117.81
645		1.033	1.016		-121.91	117.85
646		1.031	1.014		-121.98	117.90
671	0.989	1.055	0.981	-5.29	-122.35	116.22
680	0.989	1.055	0.981	-5.29	-122.35	116.22
684	0.987		0.979	-5.31		116.12
611			0.977			115.97
652	0.981			-5.24		
692	0.989	1.055	0.981	-5.30	-122.36	116.22
675	0.982	1.057	0.979	-5.54	-122.53	116.23

The CIM is an iterative solution method. The maximum error at each iteration for the three test cases introduced above is shown in Fig. 13. As can be seen, the maximum error for the 3LPF is slightly lower than the error for the CIM at its second iteration. In other words, it takes the CIM up to three iterations to exceed the accuracy of the 3LPF solution. At its first iteration, the error of the CIM is about an order of magnitude larger than the 3LPF method.

V. POTENTIAL APPLICATIONS OF THE 3LPF

While the 3LPF is directly useful in power flow analysis, its major advantages are more evident when embedded in optimization routines., where computational efficiency is of the essence. This becomes especially pressing for on-line applications that are required to produce fast and robust solutions. Distribution system state estimation (DSSE) is an important case, which has received considerable attention due to the new developments in the advanced metering infrastructure. It has been shown that the presence of unbalances can significantly affect the accuracy of the DSSE [29] and, therefore, a three-phase model of the system should be used. The DSSE has many applications in the tools provided by the modern DMS, e.g., volt-VAR control methods [30]. One of the challenges in the DSSE is the lack of sufficient measurements, which leads to an unobservable system and causes convergence issues in the DSSE algorithm. Methods have been proposed to generate pseudo-measurements to address this issue, e.g., [31]. Since the conventional power flow equations are nonlinear and non-convex, the DSSE problem is numerically intensive to solve [32]. Computational challenges arising from the inclusion of pseudo-measurements are likely to be alleviated substantially by the 3LPF method.

Another challenge in DSSE is the presence of discrete variables, e.g., status of switches, fuses, capacitor banks, and voltage regulator taps. Besides, introducing integer variables to the DSSE optimization problem creates a practically intractable problem. It is expected that the proposed 3LPF formulation paves the path for including the discrete variables within the DSSE. With the 3LPF, the resulting optimization problem can be solved using commercially available mixed-integer programming solvers. Normally, in a typical distribution feeder, there exist only a few number of voltage regulators and/or capacitor banks. Also, most of the distribution feeders are radial, which facilitates the idea of decomposing the problem into several independent sub-problems, each dealing only with a single feeder. These specific features of distribution systems make it possible to take advantage of the fast mixed-integer programming methods.

The optimal placement of new measurement devices for DSSE has been a subject of research in several studies [33], [34]. This problem can be formulated as a mixed-integer programming problem, where the existence of a measuring device can be modeled as a binary variable. The 3LPF formulation allows for the introduction of integer variables to the optimization problem of meter placement. In addition, the volt-VAR optimization problem in distribution system requires three-phase power flow analysis when voltage regulators and/or capacitor banks with single, double, and independently-operated three-phase units are present. The LPF has been successfully applied to this problem for a balanced case in [35]. The proposed 3LPF formulation can be directly applied to unbalanced cases. It should be noted that the 3LPF is still applicable even if

voltages are outside the standard limits, although the associated error may be slightly higher.

Due to the probabilistic and intermittent nature of some renewable energy resources, e.g., wind and solar, probabilistic power flow methods have been developed to find the expected value and variance of the system state variables [36], [37]. There are also elements of uncertainty in load values as well as load models in a distribution system. The proposed 3LPF is an efficient alternative to nonlinear formulations for probabilistic power flow analysis. The probabilistic power flow analysis provides a bound for the nodal voltages and branch currents for given bounds on the expected load/generation scenarios. This is useful to ensure, with some definable probability, that the system will operate within the standard limits under different scenarios. The ever-increasing penetration of distributed energy resources calls for these types of studies.

The error values reported in Section IV are acceptable for the targeted applications mentioned above.

VI. Conclusion

The current injection method for a three-phase distribution system was described and the fixed-point iteration method was used to solve the resulting power flow equations. A three-phase linear power flow (3LPF) formulation was derived based on the fact that the nodal voltages vary within a bounded range. The error associated with the 3LPF solution for various system parameters was illustrated. An important application of the 3LPF is in distribution system optimization routines, such as volt-VAR optimization, and distribution system state estimation. With this linear set of equations, it is possible to include integer variables to represent switches status, tap position for voltage regulators, etc.

Appendix A
Linear Approximation of a Two-Variable Function

Assume a nonlinear function $f(x, y)$ defined on $x \in \mathcal{D}_x$ and $y \in \mathcal{D}_y$. A linear approximation of f on the specified compact domain is $\hat{f} = K_1 x + K_2 y + K_3$. Assume N evenly distributed points in the function domain, i.e., (x_i, y_i, f_i). In order to find the best coefficients for $\hat{f}$ that closely matches f, the following least-square problem should be solved:

$$\min_{K_1,K_2,K_3} \sum_{i=1}^{N} \left(K_1 x_i + K_2 y_i + K_3 - f_i\right)^2 \tag{12}$$

Applying the Karush-Kuhn-Tucker conditions to the above problem yields the following solution:

$$\begin{bmatrix} \sum x_i^2 & \sum x_i y_i & \sum x_i \\ \sum x_i y_i & \sum y_i^2 & \sum y_i \\ \sum x_i & \sum y_i & N^2 \end{bmatrix} \begin{bmatrix} K_1 \\ K_2 \\ K_3 \end{bmatrix} = \begin{bmatrix} \sum x_i f_i \\ \sum y_i f_i \\ \sum f_i \end{bmatrix} \tag{13}$$

Note that this has to be solved for the four nonlinear functions in (9) and for each phase separately. Therefore, K_{1i}^{ph} in (10) represents K_1 for $f_i, i \in \{1, 2, 3, 4\}$, and Phase ph $\in \{A, B, C\}$.

Appendix B
Calculated K^{PH} for Linear Approximations

$$K^A = \begin{bmatrix} -0.9934 & 0 & 0.0064 & 0 \\ 0 & 0.9965 & 0 & 0.9965 \\ 1.9863 & 0 & 0.9883 & 0 \end{bmatrix}$$

$$K^B = \begin{bmatrix} 0.4991 & -0.8617 & 0.7490 & -0.4287 \\ -0.8617 & -0.4959 & -0.4287 & 0.2540 \\ -0.9932 & -1.7202 & -0.4942 & -0.8559 \end{bmatrix}$$

$$K^C = \begin{bmatrix} 0.4991 & 0.8617 & 0.7490 & 0.4287 \\ 0.8617 & -0.4959 & 0.4287 & 0.2540 \\ -0.9932 & 1.7202 & -0.4942 & 0.8559 \end{bmatrix}$$

$$K^{AB} = \begin{bmatrix} -0.1653 & -0.2872 & 0.1466 & -0.2475 \\ -0.2872 & 0.1664 & -0.2475 & 0.4324 \\ 0.9932 & 0.5734 & 0.8559 & 0.4942 \end{bmatrix}$$

$$K^{BC} = \begin{bmatrix} 0.3322 & 0 & 0.5754 & 0 \\ 0 & -0.3311 & 0 & 0.0037 \\ 0 & -1.1468 & 0 & -0.9883 \end{bmatrix}$$

$$K^{CA} = \begin{bmatrix} -0.1653 & 0.2872 & 0.1466 & 0.2475 \\ 0.2872 & 0.1664 & 0.2475 & 0.4324 \\ -0.9932 & 0.5734 & -0.8559 & 0.4942 \end{bmatrix}$$

Appendix C
Power-Flow Data for the 3-Node Test System

$Z\ (R + jX)$ is in Ω/ft; B is in μS/ft; active power P is in (MW); reactive power Q is in MVAR; lengths are in miles.

$$Z^{abc} = \begin{bmatrix} 0.651 & 0.102 & 0.104 \\ 0.102 & 0.646 & 0.100 \\ 0.104 & 0.100 & 0.649 \end{bmatrix} + j \begin{bmatrix} 0.652 & 0.282 & 0.245 \\ 0.282 & 0.663 & 0.224 \\ 0.245 & 0.224 & 0.658 \end{bmatrix}$$

$$B^{abc} = \begin{bmatrix} 2.607 & -0.748 & -0.486 \\ -0.748 & 2.491 & -0.304 \\ -0.486 & -0.304 & 2.389 \end{bmatrix}$$

$$Z^{ab} = \begin{bmatrix} 0.6 & 0.1 \\ 0.1 & 0.6 \end{bmatrix} + j \begin{bmatrix} 0.6 & 0.2 \\ 0.2 & 0.6 \end{bmatrix}, B^{ab} = \begin{bmatrix} 0 & 0 \\ 0 & 0 \end{bmatrix}$$

From	To	Load	P_a	Q_a	P_b	Q_b	P_c	Q_c	Length
1	2	Y−PQ	1	0.1	1	0.1	1	0.1	1
2	3	Y−PQ	1	0.1	1	0.1	−	−	1

References

[1] J. R. Marti, H. Ahmadi, and L. Bashualdo, "Linear power flow formulation based on a voltage-dependent load model," *IEEE Trans. Power Del.*, vol. 28, no. 3, pp. 1682–1690, Jul. 2013.

[2] H. Ahmadi and J. R. Martí, "Distribution system optimization based on a linear power flow formulation," *IEEE Trans. Power Del.*, vol. 30, no. 1, pp. 25–33, Feb. 2015.

[3] H. Ahmadi, "Linear power flow source codes," Dec. 2015 [Online]. Available: http://www.ece.ubc.ca/hameda/downloads.htm.

[4] H. L. Nguyen, "Newton-Raphson method in complex form," *IEEE Trans. Power Syst.*, vol. 12, no. 3, pp. 1355–1359, Aug. 1997.

[5] O. L. Tortelli, E. M. Lourenco, A. V. Garcia, and B. C. Pal, "Fast decoupled power flow to emerging distribution systems via complex pu normalization," *IEEE Trans. Power Syst.*, vol. 30, no. 3, pp. 1351–1358, May 2015.

[6] M. Abdel-Akher, K. M. Nor, and A. H. A. Rashid, "Improved three-phase power-flow methods using sequence components," *IEEE Trans. Power Syst.*, vol. 20, no. 3, pp. 1389–1397, Aug. 2005.
[7] I. Dzafic, H.-T. Neisius, M. Gilles, S. Henselmeyer, and V. Landerberger, "Three-phase power flow in distribution networks using Fortescue transformation," *IEEE Trans. Power Syst.*, vol. 28, no. 2, pp. 1027–1034, May 2013.
[8] M. Z. Kamh and R. Iravani, "Unbalanced model and power-flow analysis of microgrids and active distribution systems," *IEEE Trans. Power Del.*, vol. 25, no. 4, pp. 2851–2858, Oct. 2010.
[9] D. Shirmohammadi, H. W. Hong, A. Semlyen, and G. X. Luo, "A compensation-based power flow method for weakly meshed distribution and transmission networks," *IEEE Trans. Power Syst.*, vol. 3, no. 2, pp. 753–762, May 1988.
[10] C. S. Cheng and D. Shirmohammadi, "A three-phase power flow method for real-time distribution system analysis," *IEEE Trans. Power Syst.*, vol. 10, no. 2, pp. 671–679, May 1995.
[11] M. Dilek, F. De León, R. Broadwater, and S. Lee, "A robust multiphase power flow for general distribution networks," *IEEE Trans. Power Syst.*, vol. 25, no. 2, pp. 760–768, May 2010.
[12] I. Kocar, J. Mahseredjian, U. Karaagac, G. Soykan, and O. Saad, "Multiphase load-flow solution for large-scale distribution systems using MANA," *IEEE Trans. Power Del.*, vol. 29, no. 2, pp. 908–915, Apr. 2014.
[13] T.-H. Chen, M.-S. Chen, K.-J. Hwang, P. Kotas, and E. A. Chebli, "Distribution system power flow analysis—A rigid approach," *IEEE Trans. Power Del.*, vol. 6, no. 3, pp. 1146–1152, Jul. 1991.
[14] J.-H. Teng and C.-Y. Chang, "A novel and fast three-phase load flow for unbalanced radial distribution systems," *IEEE Trans. Power Syst.*, vol. 17, no. 4, pp. 1238–1244, Nov. 2002.
[15] V. M. Da Costa, N. Martins, and J. R. L. Pereira, "Developments in the Newton Raphson power flow formulation based on current injections," *IEEE Trans. Power Syst.*, vol. 14, no. 4, pp. 1320–1326, Nov. 1999.
[16] P. A. N. Garcia, J. L. R. Pereira, S. Carneiro, Jr., V. M. Da Costa, and N. Martins, "Three-phase power flow calculations using the current injection method," *IEEE Trans. Power Syst.*, vol. 15, no. 2, pp. 508–514, May 2000.
[17] T.-H. Chen and N.-C. Yang, "Loop frame of reference based three-phase power flow for unbalanced radial distribution systems," *Elect. Power Syst. Res.*, vol. 80, no. 7, pp. 799–806, 2010.
[18] P. M. De Oliveira-De Jesus, M. A. Alvarez, and J. M. Yusta, "Distribution power flow method based on a real quasi-symmetric matrix," *Elect. Power Syst. Res.*, vol. 95, pp. 148–159, 2013.
[19] A. J. Wood and B. F. Wollenberg, *Power Generation, Operation, and Control*. New York, NY, USA: Wiley, 2012.
[20] S. Bolognani and F. Dorfler, "Fast power system analysis via implicit linearization of the power flow manifold," in *Proc. 53rd Annu. Allerton Conf. Commun., Control, and Comput.*, 2015.
[21] S. Bolognani and S. Zampieri, "On the existence and linear approximation of the power flow solution in power distribution networks," *IEEE Trans. Power Syst.*, vol. 31, no. 1, pp. 163–172, Jan. 2016.
[22] L. M. Hajagos and B. Danai, "Laboratory measurements and models of modern loads and their effect on voltage stability studies," *IEEE Trans. Power Syst.*, vol. 13, no. 2, pp. 584–592, May 1998.
[23] A. Gómez-Expósito, E. Romero-Ramos, and I. Džafić, "Hybrid real-complex current injection-based load flow formulation," *Elect. Power Syst. Res.*, vol. 119, pp. 237–246, 2015.
[24] T.-H. Chen *et al.*, "Three-phase cogenerator and transformer models for distribution system analysis," *IEEE Trans. Power Del.*, vol. 6, no. 4, pp. 1671–1681, Oct. 1991.
[25] H. Ahmadi, J. R. Martí, and A. Moshref, "Piecewise linear approximation of generators cost functions using max-affine functions," in *Proc. IEEE PES General Meeting*, Vancouver, BC, Canada, 2013, pp. 1–5.
[26] *Preferred Voltage Levels for AC Systems, 0 to 50,000 V*, Std. CAN3 C235-83, Canadian Standard Association (CSA), 2010.
[27] W. H. Kersting, "Radial distribution test feeders," *IEEE Trans. Power Syst.*, vol. 6, no. 3, pp. 975–985, Aug. 1991.
[28] R. F. Arritt and R. C. Dugan, "The IEEE 8500-node test feeder," in *Proc. IEEE PES T& D Conf. Expo.*, 2010, pp. 1–6.
[29] C. W. Hansen and A. S. Debs, "Power system state estimation using three-phase models," *IEEE Trans. Power Syst.*, vol. 10, no. 2, pp. 818–824, May 1995.
[30] M. Biserica, Y. Besanger, R. Caire, O. Chilard, and P. Deschamps, "Neural networks to improve distribution state estimation-volt var control performances," *IEEE Trans. Smart Grid*, vol. 3, no. 3, pp. 1137–1144, Sep. 2012.
[31] E. Manitsas, R. Singh, B. C. Pal, and G. Strbac, "Distribution system state estimation using an artificial neural network approach for pseudo measurement modeling," *IEEE Trans. Power Syst.*, vol. 27, no. 4, pp. 1888–1896, Nov. 2012.
[32] L. Schenato, G. Barchi, D. Macii, R. Arghandeh, K. Poolla, and A. Von Meier, "Bayesian linear state estimation using smart meters and PMUs measurements in distribution grids," in *Proc. IEEE Int. Conf. Smart Grid Commun.*, 2014, pp. 572–577, IEEE.
[33] R. Singh, B. C. Pal, and R. B. Vinter, "Measurement placement in distribution system state estimation," *IEEE Trans. Power Syst.*, vol. 24, no. 2, pp. 668–675, May 2009.
[34] M. G. Damavandi, V. Krishnamurthy, and J. R. Martí, "Robust meter placement for state estimation in active distribution systems," *IEEE Trans. Smart Grid*, vol. 6, no. 4, pp. 1972–1982, Jul. 2015.
[35] H. Ahmadi, J. R. Martí, and H. W. Dommel, "A framework for volt-VAR optimization in distribution systems," *IEEE Trans. Smart Grid*, vol. 6, no. 3, pp. 1473–1483, May 2015.
[36] M. Ding and X. Wu, "Three-phase probabilistic power flow in distribution system with grid-connected photovoltaic systems," in *Proc. APPEEC*, Mar. 2012, pp. 1–6.
[37] H. Ahmadi and H. Ghasemi, "Probabilistic optimal power flow incorporating wind power using point estimate methods," in *Proc. EEEIC*, May 2011, pp. 1–5.

Hamed Ahmadi (M'15) received the B.Sc. and M.Sc. degrees in electrical engineering from the University of Tehran in 2009 and 2011, respectively, and the Ph.D. degree in electrical and computer engineering from the University of British Columbia, Vancouver, BC, Canada. He was a postdoctoral fellow at the University of British Columbia from April to August 2015, working on a joint project with BC Hydro. He is currently an Engineer at Generation and Transmission Division, BC Hydro, Burnaby, BC. His research interests include distribution systems analysis, optimization algorithms, power system stability and control, smart grids, and high voltage engineering.

José R. Martí (M'80–SM'01–F'02–LF'15) received the Electrical Engineering degree from Central University of Venezuela, Caracas, in 1971, the Master of Engineering degree in electric power (M.E.E.P.E.) from Rensselaer Polytechnic Institute, Troy, NY, in 1974, and the Ph.D. degree in electrical engineering from the University of British Columbia, Vancouver, BC, Canada in 1981. He is known for his contributions to the modeling of fast transients in large power networks, including component models and solution techniques. Particular emphasis in recent years has been the development of distributed computational solutions for real-time simulation of large systems and integrated multisystem solutions. He is a Professor of electrical and computer engineering at the University of British Columbia and a Registered Professional Engineer in the Province of British Columbia, Canada.

Alexandra "Sascha" von Meier (M'12) received a B.A. in physics in 1986 and a Ph.D. in energy and resources in 1995 from University of California at Berkeley. She is presently an Adjunct Professor in the Department of Electrical Engineering and Computer Science at UC Berkeley, and Director of Electric Grid Research at the California Institute for Energy and Environment (CIEE). Her research focuses on Smart Grid issues, the use of advanced sensing and monitoring capabilities such as synchrophasor data for power distribution systems, and the integration of renewable resources. She was previously a professor of energy management and design at Sonoma State University.